




## Synthesis and characterization of ruthenium(II) hydrazone complexes as anticancer chemotherapeutic agents: in vitro DNA/BSA protein binding and cytotoxicity assay

E. Jayanthi, M. Anusuya, N.S.P. Bhuvanesh, K.A. Khalil & N. Dharmaraj


To cite this article: E. Jayanthi, M. Anusuya, N.S.P. Bhuvanesh, K.A. Khalil & N. Dharmaraj (2015) Synthesis and characterization of ruthenium(II) hydrazone complexes as anticancer chemotherapeutic agents: in vitro DNA/BSA protein binding and cytotoxicity assay, Journal of Coordination Chemistry, 68:20, 3551-3565, DOI: [10.1080/00958972.2015.1077950](https://doi.org/10.1080/00958972.2015.1077950)

To link to this article: <http://dx.doi.org/10.1080/00958972.2015.1077950>

 View supplementary material 

 Accepted author version posted online: 31 Jul 2015.  
Published online: 25 Aug 2015.

 Submit your article to this journal 

 Article views: 161

 View related articles 

 View Crossmark data 

## Synthesis and characterization of ruthenium(II) hydrazone complexes as anticancer chemotherapeutic agents: *in vitro* DNA/BSA protein binding and cytotoxicity assay

E. JAYANTHI<sup>†</sup>, M. ANUSUYA<sup>†</sup>, N.S.P. BHUVANESH<sup>‡</sup>, K.A. KHALIL<sup>§¶</sup> and N. DHARMARAJ<sup>\*†</sup>

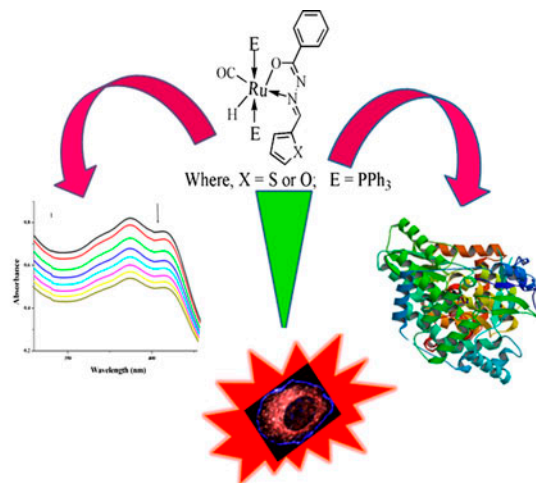
<sup>†</sup>Inorganic & Nanomaterials Research Laboratory, Department of Chemistry, Bharathiar University, Coimbatore, India

<sup>‡</sup>Department of Chemistry, Texas A&M University, College Station, TX, USA

<sup>§</sup>Department of Mechanical Engineering, College of Engineering, King Saud University, Riyadh, Saudi Arabia

<sup>¶</sup>Faculty of Energy Engineering, Aswan University, Aswan, Egypt

(Received 4 February 2015; accepted 30 June 2015)



Ruthenium hydrazone complexes  $[\text{RuH}(\text{CO})(\text{L}^1)(\text{PPh}_3)_2]$  (**1**) and  $[\text{RuH}(\text{CO})(\text{L}^2)(\text{PPh}_3)_2]$  (**2**) synthesized by reacting  $[\text{RuHCl}(\text{CO})(\text{PPh}_3)_3]$  with benzoic acid[(thiophene-2-yl)methylene]hydrazide ( $\text{HL}^1$ ) or benzoic acid[1-(furan-2-yl)methylene]hydrazide ( $\text{HL}^2$ ) were characterized by elemental analysis, IR spectral, and XRD techniques. An intercalative interaction of the free ligands as well as **1** and **2** with CT-DNA was identified through absorption/emission titrations and viscosity measurements. Their bovine serum albumin binding through absorption/emission and synchronous spectral studies indicated significant binding proficiency. *In vitro* cytotoxic study of the complexes carried out against HeLa and MCF7 cell lines demonstrated that both complexes are potentially cytotoxic against both cell lines. The superior biological potential of **1** compared to **2** was attributed to the presence of sulfur containing heterocyclic moiety in the former complex.

\*Corresponding author. Email: [dharmaraj@buc.edu.in](mailto:dharmaraj@buc.edu.in)

**Keywords:** Heterocyclic hydrazones; Ru(II) complex; DNA/Protein binding; Cytotoxicity; Triphenylphosphine

## 1. Introduction

With the serendipitous discovery of cisplatin, platinum anticancer drugs made coordination chemistry an active research field. Their clinical success limited by several side effects [1] provoked many researchers to probe other metal-based drug candidates with potential anti-cancer properties but with less toxicity. Ruthenium complexes were identified as one of the alternate classes due to their stability, iron mimicking property, and structural novelty [2–4]. In particular, NAMI-A and KP1019 are in various stages of clinical trials [5, 6]. Generally, DNA is the primary intracellular target of anticancer drugs. Interaction between small molecules and DNA can often manipulate biodistribution, DNA binding rate and mode, as well as recognition by DNA-repair mechanisms, causing damage to cancer cells, blocking the division of cancer cells, and even death of cancer cells [7]. Thus, it was thought worthwhile to study the interaction of metal-based drugs with DNA for a better understanding of their pharmacological properties to design new therapeutic agents [8]. Serum albumin has long been the center of attention of the pharmaceutical industry due to its ability to bind with various drug molecules and alter the overall distribution, metabolism, and efficacy of many drugs based on their affinity to serum albumin [9, 10]. Bovine serum albumin (BSA) is the most extensively studied protein due to its structural resemblance with human serum albumin and hence, it was chosen as model protein to study the drug–albumin interaction.

Metal complexes with hydrazones play an important role in enhancing the biological activity of free hydrazones [11, 12]. Owing to the wide range of applications of ruthenium complexes [13], there is a continuous interest in new complexes with enhanced activities. Hence, we report the synthesis of ruthenium(II) carbonyl complexes **1** and **2** by reacting  $[\text{RuHCl}(\text{CO})(\text{PPh}_3)_3]$  with benzoic acid[(thiophene-2-yl)methylene] hydrazide ( $\text{HL}^1$ ) or benzoic acid[1-(furan-2-yl)methylene] hydrazide ( $\text{HL}^2$ ) along with their structural characterization. Interaction of **1** and **2** with calf-thymus DNA (CT-DNA) and BSA has been analyzed by absorption/emission titrations and viscosity measurements.

## 2. Experimental

### 2.1. Materials and methods

$\text{RuCl}_3 \cdot 3\text{H}_2\text{O}$  was purchased from Loba-Chemie and used as received.  $[\text{RuHCl}(\text{CO})(\text{PPh}_3)_3]$  and the ligands ( $\text{HL}^1$  and  $\text{HL}^2$ ) were prepared according to the literature methods [14, 15]. Protein free CT-DNA obtained from Sigma-Aldrich Chemicals was stored at 0–4 °C, and its purity was checked by measuring its optical density before use. Doubly distilled water was used to prepare Tris–HCl buffer (5 mM Tris–HCl, 50 mM NaCl, pH 7.2). DNA stock solutions were freshly prepared before use with this buffer solution. Ethidium bromide (EB) and 3-(4,5-dimethylthiazol-2-yl)-2,5-diphenyltetrazolium bromide (MTT) were purchased from Sigma-Aldrich and used as received.

Elemental analyses (C, H, N, and S) were performed on a Vario EL III Elemental analyzer. IR spectra (4000–400  $\text{cm}^{-1}$ ) of the samples were recorded as KBr disks using a Nicolet Avatar Model FT-IR spectrophotometer. Electronic absorption spectra were recorded

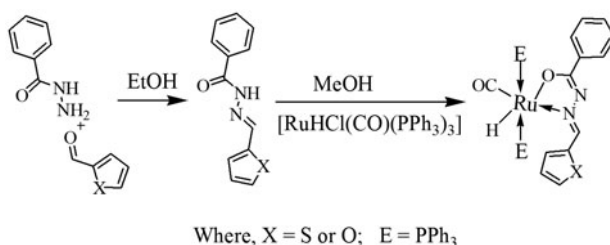


Figure 1. Synthetic scheme of HL<sup>1</sup>, HL<sup>2</sup>, **1**, and **2**.

with a Jasco V-630 spectrophotometer. Emission spectra of the ligands and complexes were recorded by a Jasco FP 6600 spectrofluorometer. Viscosity experiments were carried out using a semi-microviscometer maintained at 27(±0.1) °C in a thermostatic bath. Human cervical cancer cells (HeLa) and human breast cancer cells (MCF-7) were obtained from National Center for Cell Science, Pune, India.

## 2.2. Preparation of ligands HL<sup>1</sup> and HL<sup>2</sup>

HL<sup>1</sup> and HL<sup>2</sup> were synthesized by condensing equimolar amounts of benzhydrazide (0.6805 g, 5 mM) with thiophene carbaldehyde (0.5605 g, 5 mM) or furfuraldehyde (0.4805 g, 5 mM) in methanol (50 mL) according to the literature method (figure 1).

## 2.3. Synthesis of ruthenium(II) hydrazone complexes [RuH(CO)(PPh<sub>3</sub>)<sub>2</sub>(L<sup>1</sup>)] (**1**) and [RuH(CO)(PPh<sub>3</sub>)<sub>2</sub>(L<sup>2</sup>)] (**2**)

Ruthenium complexes **1** and **2** were prepared by the following general procedure (figure 1). A solution of HL<sup>1</sup> (0.230 g, 1 mM) or HL<sup>2</sup> (0.214 g, 1 mM) in 20 mL warm methanol was added to [RuHCl(CO)(PPh<sub>3</sub>)<sub>3</sub>] (0.917 g, 1 mM) in methanol, refluxed for 48 h and kept at room temperature for crystallization. Red needle-like crystals of **1** suitable for X-ray studies were obtained after slow evaporation of the reaction mixture over a week. Our attempts to isolate crystals of **2** for single crystal XRD studies were unsuccessful.

**[Ru(H)(CO)(PPh<sub>3</sub>)<sub>2</sub>(L<sup>1</sup>)]** (**1**). Yield: 61%. Melting point: 200 °C. Anal. Calcd for C<sub>49</sub>H<sub>40</sub>N<sub>2</sub>O<sub>2</sub>P<sub>2</sub>RuS (MW = 883.90): C, 66.57; H, 4.56; N, 3.16; S, 3.62 (%). Found: C, 66.71; H, 4.68; N, 3.22; S, 3.73. UV-vis (solvent: DMSO-Tris-HCl buffer); λ<sub>max</sub>: nm (ε/M<sup>-1</sup> cm<sup>-1</sup>): 271(33,836), 387(21,579), 407(19,863); Selected IR bands (KBr, in cm<sup>-1</sup>): 1580, 1495 (>C = N-N = C<); 1387 (C-O); 1089 (N-N); 2020 (Ru-H); 1945 (Ru-CO).

**[Ru(H)(CO)(PPh<sub>3</sub>)<sub>2</sub>(L<sup>2</sup>)]** (**2**). Yield: 58%. Melting point: 222 °C. Anal. Calcd for C<sub>49</sub>H<sub>40</sub>N<sub>2</sub>O<sub>3</sub>P<sub>2</sub>Ru (MW = 867.90): C, 67.81; H, 4.64; N, 3.22 (%). Found: C, 67.92; H, 4.69; N, 3.28. UV-vis (solvent: DMSO-Tris-HCl buffer); λ<sub>max</sub>: nm (ε/M<sup>-1</sup> cm<sup>-1</sup>): 272 (32,915), 380(15,685), 404(13,574). Selected IR bands (KBr, in cm<sup>-1</sup>): 1579, 1493 (>C = N-N = C<); 1384 (C-O); 1092 (N-N); 2025 (Ru-H); 1946 (Ru-CO).

## 2.4. Crystal structure determination

The X-ray diffraction data of **1** were determined by a BRUKER APEX 2 X-ray (three-circle) diffractometer using graphite monochromated Mo-Kα radiation (λ = 0.71073 Å)

initiated using  $\omega$  and  $\varphi$  scans. Integrated intensity information for each reflection was obtained by using APEX2 [16]. SADABS [17] was employed to correct the data for absorption effects. X-ray data reduction and structure solution were done using SHELXTL (XS) [18]. Hydrogens were placed using riding models. All non-hydrogen atoms were refined with anisotropic thermal parameters. The structure was refined (weighted least squares refinement on  $F^2$ ) to convergence. Olex2 was employed for the final data presentation and structure plots [19].

## 2.5. DNA binding experiments

**2.5.1. Absorption titration.** To identify the mode of interaction of HL<sup>1</sup>, HL<sup>2</sup>, **1**, and **2** with CT-DNA, UV-vis spectra of CT-DNA in the presence and absence of each compound were recorded for constant concentration of the compound (25  $\mu\text{M}$ ) and varying CT-DNA concentration (2.5–20  $\mu\text{M}$ ). The concentration of CT-DNA was determined by its UV absorbance at 260 nm. Solutions of CT-DNA in Tris-HCl buffer gave a ratio of UV absorbance at 260 and 280 nm,  $A_{260}/A_{280}$ , of approximately 1.9 indicating that the DNA was sufficiently free of protein [20]. The molar absorption coefficient at 260 nm,  $\epsilon_{260}$  was taken as 6600  $\text{M}^{-1} \text{cm}^{-1}$  [21]. Control experiments with DMSO were performed and no changes in the spectra of CT-DNA were observed. The magnitude of the binding strength ( $K_b$ ) of the ligands and complexes with CT-DNA is estimated by the equation (1):

$$[\text{DNA}]/(\epsilon_a - \epsilon_f) = [\text{DNA}]/(\epsilon_b - \epsilon_f) + 1/K_b(\epsilon_b - \epsilon_f) \quad (1)$$

where [DNA] is the concentration of DNA, and  $\epsilon_a$ ,  $\epsilon_f$ , and  $\epsilon_b$  correspond to the extinction coefficient for the free compound, compound in the presence of DNA, and compound in fully bound form, respectively. In plots of  $[\text{DNA}]/(\epsilon_a - \epsilon_f)$  versus [DNA],  $K_b$  is given by the ratio of slope to intercept [22].

**2.5.2. Luminescence titration in the presence of EB.** Competitive interaction of the ligands and complexes with EB has been investigated by fluorescence spectroscopy. The fluorescence spectra of DNA bound EB were obtained in the excitation ( $\lambda_{\text{ex}}$ ) and the emission ( $\lambda_{\text{em}}$ ) wavelengths of 515 and 602 nm, respectively, by keeping the concentration of CT-DNA (5  $\mu\text{M}$ ) in buffer-EB (5  $\mu\text{M}$ ) as constant and adding small aliquots of ligands and Ru(II) complex solutions (5–30  $\mu\text{M}$ ). The quenching of EB bound to DNA by the compounds is in agreement with the linear Stern-Volmer equation [22]:

$$I_0/I = 1 + K_{\text{SV}}[Q] \quad (2)$$

where  $I_0$  is the emission intensity in the absence of the quencher,  $I$  is the emission intensity in the presence of the quencher,  $K_{\text{SV}}$  is the Stern-Volmer quenching constant, and  $[Q]$  is the quencher concentration. The  $K_{\text{SV}}$  value is obtained as a slope from the plot of  $I_0/I$  versus  $[Q]$ .

**2.5.3. Viscosity measurements.** For viscosity measurements, DNA samples (0.5 mM) were prepared by sonication in order to minimize complexities arising from DNA flexibility

[23]. The flow time of each sample was measured three times with a digital stopwatch and an average flow time was calculated. Relative viscosities for DNA in the presence and absence of complex were calculated from the relationship  $\eta = (t - t^0)/t^0$ , where  $t$  is the observed flow time of the DNA-containing solution and  $t^0$  is the flow time of the buffer alone. The data were presented as  $(\eta/\eta^0)^{1/3}$  versus the binding ratio, where  $\eta$  and  $\eta^0$  are the specific viscosities of DNA in the presence and absence of the test compounds, respectively [24].

## 2.6. BSA binding studies

The excitation wavelength of BSA at 280 nm and quenching of the emission intensity of tryptophan residues of BSA at 345 nm were monitored using constant concentration of BSA (1  $\mu\text{M}$ ) but with increasing concentration of complexes (2–12  $\mu\text{M}$ ) [12]. The excitation and emission slit widths and scan rates were kept constant. A concentrated stock solution of the compounds was prepared in DMSO and suitably diluted with phosphate buffer to the concentration required for all of the experiments. Synchronous fluorescence spectra were also recorded using the same concentration of BSA and complexes as mentioned above with two different  $\Delta\lambda$  (difference between the excitation and emission wavelengths of BSA) values such as 15 and 60 nm at which the spectrum only shows the spectroscopic behavior of either tyrosine or tryptophan residues of BSA, respectively. Stern–Volmer and Scatchard graphs were used to study the interaction of the quencher with serum albumins. According to the Stern–Volmer quenching equation [12]:

$$I_0/I = 1 + k_q\tau_0[Q] = 1 + K_{SV}[Q] \quad (3)$$

where  $I_0$  is the initial tryptophan fluorescence intensity of BSA,  $I$  is the tryptophan fluorescence intensity of BSA after addition of the quencher,  $k_q$  is the quenching rate constant of protein,  $K_{SV}$  is the Stern–Volmer quenching constant,  $\tau_0$  is the average lifetime of BSA without the quencher, and  $[Q]$  is the concentration of the quencher, respectively.

## 2.7. Cytotoxic studies

*In vitro* growth inhibitory effects of **1** and **2** toward HeLa and MCF-7 cell lines were evaluated by MTT (tetrazolium salt reduction) assay [25] with cells grown in Eagle's minimum essential medium containing 10% fetal bovine serum (FBS). For the screening experiment, the cells were seeded into 96-well plates containing 10% FBS, at a plating density of 10,000 cells/well and incubated at 37 °C, under conditions of 5% CO<sub>2</sub>, 95% air, and 100% relative humidity for 24 h prior to the addition of compounds. Cells were treated with different concentrations of ruthenium complexes (1–100  $\mu\text{M}$ ) for 48 h. The medium without the compounds served as the control. After 48 h, 10  $\mu\text{L}$  of MTT (5 mg mL<sup>-1</sup>) in phosphate-buffered saline was added to each well and incubated at 37 °C for 4 h. The medium containing MTT was removed and formazan crystals were dissolved in DMSO. IC<sub>50</sub> values represent the drug concentrations that reduced the mean absorbance at 570 nm to 50% of those in the untreated control wells, and a graph was plotted with the percentage of cell inhibition versus concentration to calculate the IC<sub>50</sub> value.

$$\% \text{ Inhibition} = [\text{mean OD of untreated cells (control)} / \text{mean OD of treated cells}] \times 100 \quad (4)$$

### 3. Results and discussion

#### 3.1. Synthesis and characterization

Reactions of  $[\text{RuHCl}(\text{CO})(\text{PPh}_3)_3]$  with  $\text{HL}^1$  and  $\text{HL}^2$  yielded air stable, mononuclear octahedral complexes  $[\text{RuH}(\text{CO})(\text{PPh}_3)_2(\text{L}^1)]$  (**1**) and  $[\text{RuH}(\text{CO})(\text{PPh}_3)_2(\text{L}^2)]$  (**2**) (figure 1). The analytical data of the complexes are in agreement with the proposed molecular formulas and the complexes are soluble in common organic solvents.

Electronic spectra of the ligands, **1**, and **2** recorded in DMSO:buffer solution exhibited two/three bands from 210 to 500 nm. The UV spectrum of the ligand showed two bands below 330 nm that are attributed to  $\pi \rightarrow \pi^*$  and  $n \rightarrow \pi^*$  transitions of the ligands. In the case of complexes, the bands around 360–410 nm were assigned to charge-transfer transitions based on their extinction coefficient values, and the higher energy bands below 330 nm are attributable to  $\pi \rightarrow \pi^*$  and  $n \rightarrow \pi^*$  intraligand transitions [26, 27]. IR spectra of the ligands exhibited characteristic absorption bands at 3244/3250, 1652/1650, 1570/1579, and 1057/1057  $\text{cm}^{-1}$  due to  $\nu_{(\text{N-H})}$ ,  $\nu_{(\text{C=O})}$ ,  $\nu_{(\text{C=N})}$ , and  $\nu_{(\text{N-N})}$  vibrations, respectively, for  $\text{HL}^1/\text{HL}^2$ . In spectra of **1** and **2**, bands due to  $\nu_{(\text{C=O})}$  and  $\nu_{(\text{N-H})}$  stretches were absent and two new bands appeared between 1495/1493 and 1387/1384  $\text{cm}^{-1}$  due to the  $\nu_{(\text{C=N-N=C})}$  and  $\nu_{(\text{C-O})}$  stretching vibrations, respectively, from enolization and deprotonation of the ligands prior to coordination. The decrease in  $\nu_{(\text{C=N})}$  indicated coordination of imine-nitrogen to ruthenium [28, 29]. Appearance of bands from 2020/2025 and at 1945/1946  $\text{cm}^{-1}$  suggested the presence of Ru–H and terminally coordinated carbon monoxide (Ru–CO) [26] in both complexes.

#### 3.2. Crystal structure of $[\text{RuH}(\text{CO})(\text{PPh}_3)_2(\text{L}^1)]$ (**1**)

Molecular structure of **1** is depicted along with the atom labeling scheme in figure S1. The crystallographic data and pertinent bond lengths and angles are listed in tables 1 and 2, respectively.

Complex **1** crystallized into a monoclinic lattice with space group  $P_2(1)/n$  featuring the coordination of  $\text{HL}^1$  to ruthenium forming a five-membered chelate ring. Ruthenium is in a distorted octahedral geometry in which the imine-N and deprotonated amide-O donors of hydrazone, a hydride ion, and a carbon monoxide completed the planar base around the metal center. As commonly observed for six-coordinate complexes containing the  $\{\text{Ru}(\text{PPh}_3)_2\}$  unit, two bulky  $\text{PPh}_3$  molecules are present in axial positions. Ru–P bond lengths are much longer Ru1–P1/P2 [2.342 Å/2.351 Å] than the four equatorial bond lengths [1.769–2.162 Å], indicating axial distortion. These bond lengths are essentially equivalent and comparable to those in other related complexes [30, 31]. In addition, the strong *trans* effect of  $\text{PPh}_3$  could also account for the bond lengthening. The +2 oxidation state of the metal center is compensated by coordination of deprotonated amide carbonyl of  $\text{HL}^1$  and a hydride. The *trans* angle of P1–Ru1–P2 [163.45°] is not close to the ideal value of 180° due to axial distortion. Other *trans* angles of the basal planes, O1–Ru1–H1 [161.45°] and N1–Ru1–C49 [172.79°], also showed distortion from regular octahedral angles. The *cis* bond angles are from acute to obtuse of 74.94(7)°–100°. The observed bond lengths of

Table 1. Experimental data for crystallographic analysis of **1**.

CCDC deposition No.	1024327
Empirical formula	C <sub>49</sub> H <sub>40</sub> N <sub>2</sub> O <sub>2</sub> P <sub>2</sub> RuS
Formula weight	883.90
Temperature (K)	110(2)
Wavelength (Å)	0.71073
Crystal system	Monoclinic
Space group	<i>P</i> <sub>2</sub> (1)/ <i>n</i>
Unit cell dimensions	
<i>a</i> (Å)	12.4357(19)
<i>b</i> (Å)	17.191(3)
<i>c</i> (Å)	19.528(3)
$\alpha$ (°)	90(10)
$\beta$ (°)	100.081(2)
$\gamma$ (°)	90
Volume (Å <sup>3</sup> )	4110.3(11)
<i>Z</i>	4
Density (calculated) (Mg m <sup>-3</sup> )	1.428
Abs.coefficient (mm <sup>-1</sup> )	0.553
<i>F</i> (000)	1816
Crystal size (mm <sup>3</sup> )	0.21 × 0.20 × 0.14
Reflections collected	45,915
Independent reflections	9405 [ <i>R</i> (int) = 0.0415]
Goodness-of-fit on <i>F</i> <sup>2</sup>	1.025
Final <i>R</i> indices [ <i>I</i> > 2 $\sigma$ ( <i>I</i> )]	<i>R</i> 1 = 0.0354, <i>wR</i> 2 = 0.0878
<i>R</i> indices (all data)	<i>R</i> 1 = 0.0432, <i>wR</i> 2 = 0.0936

Table 2. Selected bond lengths (Å) and angles (°) of **1**.

Bond lengths	(Å)	Bond angles	(°)
Ru1–N1	2.104	C49–Ru1–H1	99.93
Ru1–O1	2.162	O1–Ru1–N1	74.94
Ru1–P1	2.342	C49–Ru1–O1	98.57
Ru1–P2	2.351	H1–Ru1–N1	86.67
Ru1–H1	1.769	C49–Ru1–N1	172.79
Ru1–C49	1.861	H1–Ru–O	161.45
N2–C1	1.319	P1–Ru1–P2	163.45
C8=N1	1.295	C49–Ru1–P1	91.32

Ru1–O1, Ru1–N1, Ru1–H1, and Ru1–C49 are comparable with the values reported for ruthenium complexes [31, 32].

### 3.3. DNA binding studies

**3.3.1. Absorption spectroscopic measurements.** Figure 2 shows the absorption spectra of ligands and complexes in the presence and absence of increasing concentration of DNA. On the titration of CT-DNA with the test compounds, the band of the corresponding free ligands HL<sup>1</sup>/HL<sup>2</sup>, **1**, and **2** at 312, 320, 387, and 380 nm exhibited hypochromism of 18.7, 17.4, 34.6, and 34.0%, with bathochromic shift of 1, 1, 2, and 3 nm, respectively. The intrinsic constants *K*<sub>b</sub> were determined by monitoring the changes in the absorbance of the aforementioned bands. The values of *K*<sub>b</sub> were determined (figure S2) to be 5.3(±0.2) ×



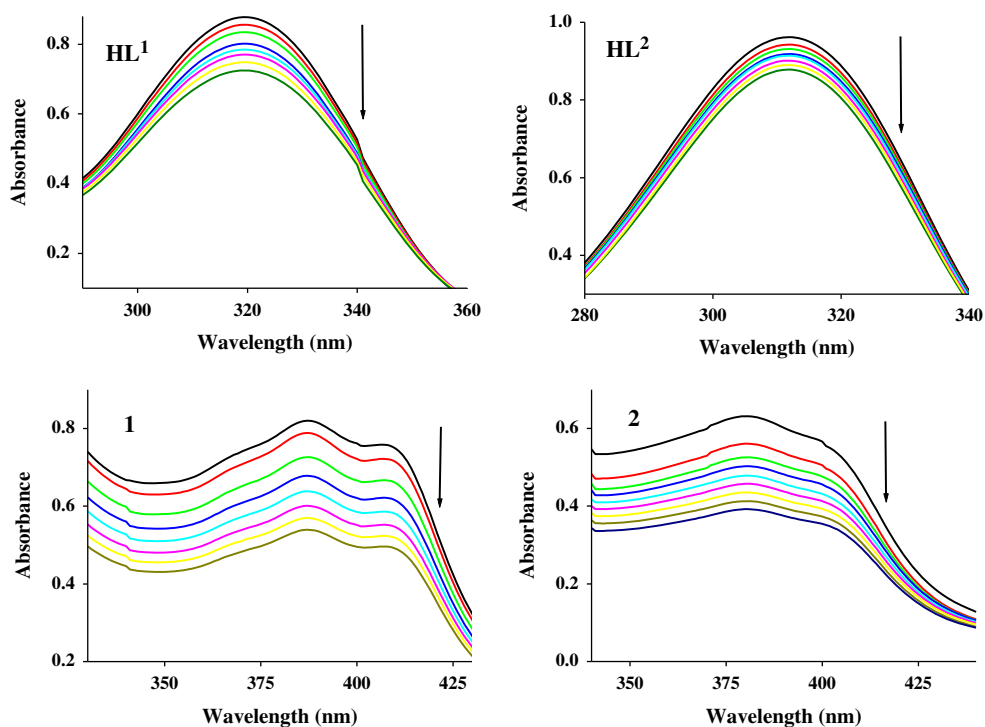


Figure 2. Electronic spectra of HL<sup>1</sup>, HL<sup>2</sup>, **1**, and **2** (25  $\mu\text{M}$ ) in the absence and presence of increasing amounts of CT-DNA (2.5, 5.0, 7.5, 10.0, 12.5, 15.0, 17.5, and 20.0  $\mu\text{M}$ ). The arrow shows the changes in absorbance with respect to an increase in the DNA concentration.

$10^4 \text{ M}^{-1}$ ,  $2.8(\pm 0.2) \times 10^3 \text{ M}^{-1}$ ,  $8.9(\pm 0.2) \times 10^4 \text{ M}^{-1}$ , and  $1.5(\pm 0.3) \times 10^4 \text{ M}^{-1}$  for HL<sup>1</sup>, HL<sup>2</sup>, **1**, and **2**, respectively. The spectral characteristics and observed values of  $K_b$  suggest that the compounds interact with DNA through intercalation between the aromatic chromophore and the base pairs of DNA [33]. The binding constants of the complexes are higher than that of the corresponding ligands and are comparable to those reported earlier for metallointercalators such as  $[\text{Ru}(\text{phen})_2(\text{dmdppz})(\text{ClO}_4)_2]$  ( $6.89 \times 10^4 \text{ M}^{-1}$ ) [2] and  $[\text{RuH}(\text{CO})(\text{PPh}_3)_2(\text{L})]$  ( $4.1(\pm 0.5) \times 10^4 \text{ M}^{-1}$ ) [12] and are lower than that of  $[\text{Ru}(\text{dmb})_2(\text{addppn})(\text{ClO}_4)_2]$  ( $4.8(\pm 0.5) \times 10^5 \text{ M}^{-1}$ ) [3]. From the absorption spectral study, it is clear that the complex formation enhances the DNA binding capability [11, 12].

**3.3.2. Competitive binding between EB and compounds for CT-DNA.** Fluorescence of CT-DNA-EB complex can be quenched by the addition of a second DNA binding molecule [34]. The fluorescence emission spectra of EB bound to DNA in the absence and presence of HL<sup>1</sup>, HL<sup>2</sup>, **1**, and **2** are shown in figure 3.

Upon addition of compounds to CT-DNA pre-treated with EB, 23.9, 22.6, 34.3, and 33.2%, reduction in the emission intensity accompanied by 2, 1, 7, and 1 nm bathochromic shift of the band around 610 nm was observed as a result of replacement of the EB fluorophore by respective compounds. The quenching magnitudes of the test compounds calculated using slope of the plot of  $I_0/I$  versus  $[Q]$  (figure S3) provided the  $K_{sv}$  values 1.0

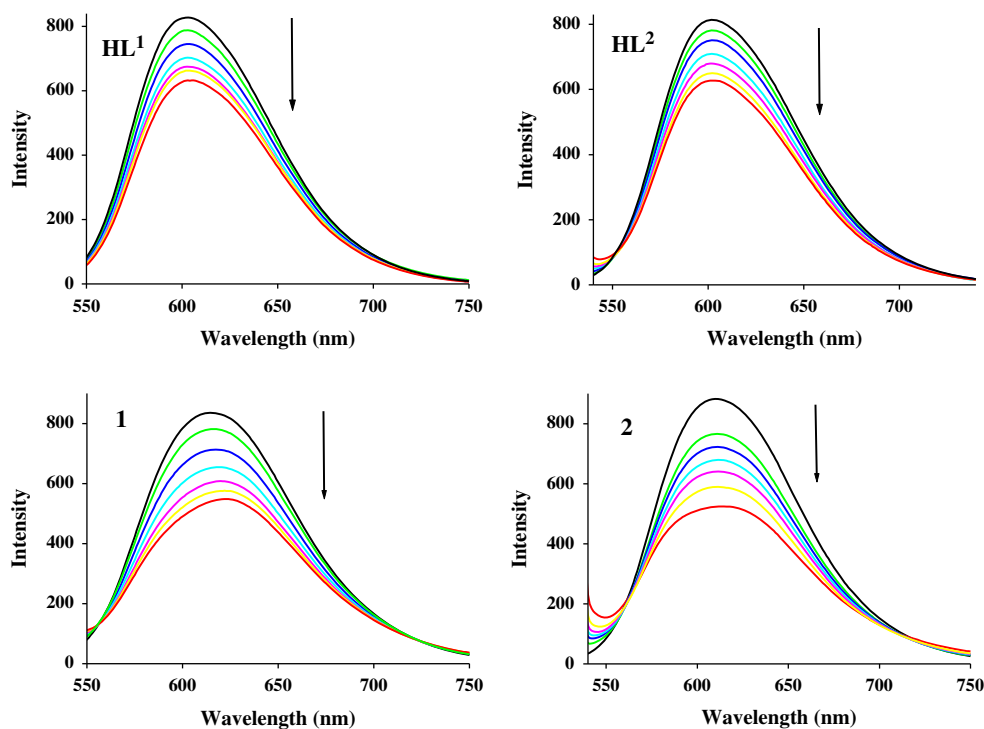


Figure 3. Emission spectra of DNA-EB in the presence of 0, 5, 10, 15, 20, 25, and 30  $\mu\text{M}$  of HL<sup>1</sup>, HL<sup>2</sup>, **1**, and **2**. The arrow indicates the changes in the emission intensity as a function of complex concentration.

$(\pm 0.2) \times 10^4 \text{ M}^{-1}$ ,  $9.9(\pm 0.4) \times 10^3 \text{ M}^{-1}$ ,  $2.5(\pm 0.3) \times 10^4 \text{ M}^{-1}$ , and  $1.6(\pm 0.5) \times 10^4 \text{ M}^{-1}$  for HL<sup>1</sup>, HL<sup>2</sup>, **1**, and **2**, respectively. These values are comparable with that of  $[\text{Ru}(\text{L}1)(\text{bpy})_2]\text{ClO}_4$  [35]. Furthermore, the apparent DNA binding constants ( $K_{\text{app}}$ ) were calculated using equation (5),

$$K_{\text{EB}}[\text{EB}] = K_{\text{app}}[\text{complex}] \quad (5)$$

where [complex] is the concentration of the complex at 50% quenching of DNA bound EB emission intensity,  $K_{\text{EB}}$  ( $1.0 \times 10^7 \text{ M}^{-1}$ ) is the DNA binding constant of EB, [EB] is the concentration of EB = 5  $\mu\text{M}$ .  $K_{\text{app}}$  values were found to be  $4.9(\pm 0.2) \times 10^5 \text{ M}^{-1}$ ,  $1.0(\pm 0.4) \times 10^5 \text{ M}^{-1}$ ,  $1.1(\pm 0.3) \times 10^6 \text{ M}^{-1}$ , and  $8.9(\pm 0.5) \times 10^5 \text{ M}^{-1}$  for HL<sup>1</sup>, HL<sup>2</sup>, **1** and **2**, respectively. The observed experimental data suggested that **1** replaced the EB more effectively than **2** and the ligands. The results are in agreement with the absorption spectroscopic measurements.

**3.3.3. Viscosity measurements.** Lengthening of the DNA double helix through intercalation by a compound normally results in an increase in the viscosity of DNA solutions [36], whereas a reduction in the relative viscosity is typically observed with covalent DNA binding [37]. Viscometric titrations were performed by increasing the concentration of

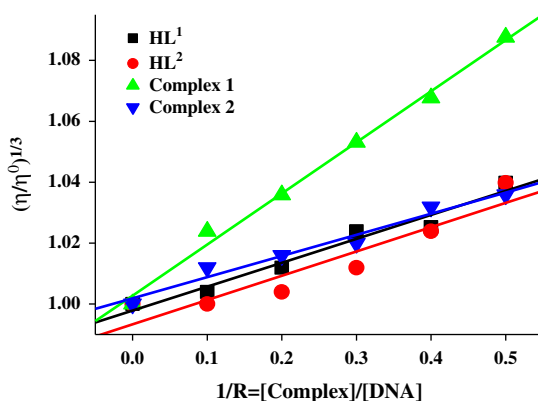


Figure 4. Variation in the viscosity of CT-DNA ( $1 \mu\text{M}$ ) upon addition of  $\text{HL}^1$ ,  $\text{HL}^2$ , **1**, and **2**.

complexes ( $0.1 \times 10^{-7}$ – $0.5 \times 10^{-7}$  M) to DNA ( $1 \times 10^{-6}$  M). The values of relative specific viscosities of CT-DNA in the absence and presence of the compounds are plotted against  $[\text{complex}]/[\text{DNA}]$  ratio (figure 4). From figure 4, a steady increase in the viscosity of DNA was observed as a function of concentration of test compounds revealing an intercalative mode of binding between the biomolecule and test compounds [38].

### 3.4. Protein binding studies

**3.4.1. Fluorescence quenching measurements.** Fluorescence quenching measurements are widely used to study the interaction of inorganic compounds with proteins [39]. This method reveals the accessibility of quenchers to protein fluorophores and helps to understand protein-binding mechanisms. From figure 5, it is clear that the addition of **1** and **2** to BSA resulted in the reduction in emission intensity of BSA fluorescence by 37.54 and

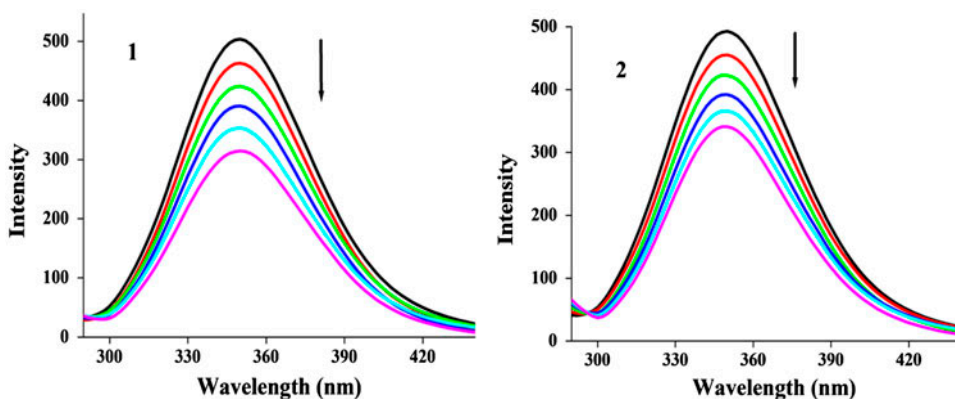


Figure 5. Emission spectra of BSA ( $1 \times 10^{-6}$  M;  $\lambda_{\text{exci}} = 280$  nm;  $\lambda_{\text{em}} = 345$  nm) as a function of concentration of **1** and **2** ( $2, 4, 6, 8, 10,$  and  $12 \times 10^{-6}$  M). The arrow indicates the effect of metal complexes on the fluorescence emission of BSA.

30.8%, respectively, with a blue-shift of 2 nm. Blue-shift is chiefly due to the burial of active sites in hydrophobic location. The magnitude of Stern–Volmer quenching constant  $K_{SV}$  obtained from the plot of  $I_0/I$  versus  $[Q]$  (figure S4) was  $6.3(\pm 0.2) \times 10^5$  and  $4.5(\pm 0.3) \times 10^5 \text{ M}^{-1}$  with respect to **1** and **2**; these values are higher than reported in the case of  $[\text{Ru}(\text{L1})(\text{bpy})_2]\text{ClO}_4$  [35]. Fluorescence reduction, observed shift, and quenching constant values suggested interaction of complexes with the protein.

**3.4.2. Absorption spectral technique.** Figure 6 shows the absorption spectra of BSA in the presence and absence of **1** and **2**. The absorption band obtained for BSA at 278 nm showed a significant increase in absorbance by the addition of **1** and **2** revealing that there exists a static interaction between BSA and the complexes due to the formation of ground-state complexes of the type reported earlier [40].

**3.4.3. Calculation of binding sites and equilibrium binding constants.** Equilibrium binding constants and number of binding sites are analyzed using Scatchard equation [40],

$$\log[(F_0 - F)/F] = \log[K] + n \log[Q] \quad (6)$$

where  $K$  and  $n$  are the binding constant and the number of binding sites, respectively. From plots of  $\log[(F_0 - F)/F]$  versus  $\log[Q]$  (figure S5), the magnitude of binding constants of **1** and **2** were calculated to be  $3.3(\pm 0.2) \times 10^5$  and  $7.4(\pm 0.3) \times 10^4 \text{ M}^{-1}$ , respectively, and are comparable to that of Ru(II) triphenylphosphine complexes [12, 41]. The number of binding sites available for **1** and **2** was 1.1555 and 1.0458, respectively. The magnitude of binding interaction of the complexes is high enough to attach with BSA and also quite below the value of association constant of non-covalent interaction between avidin and ligands ( $K \approx 10^{15} \text{ M}^{-1}$ ), suggesting that they can be easily stored in protein and released at desired target areas [42, 43].

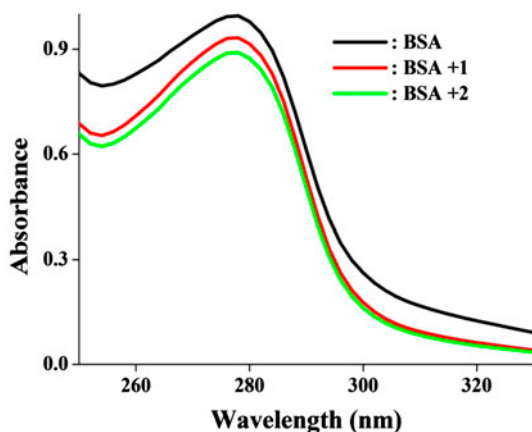


Figure 6. Absorption spectra of BSA ( $1 \times 10^{-5} \text{ M}$ ), BSA-complex **1** (BSA =  $1 \times 10^{-5}$  and **1** =  $1 \times 10^{-6} \text{ M}$ ) and BSA, **2**.

**3.4.4. Synchronous fluorescence spectra.** Synchronous fluorescence spectrum provides evidence on the molecular microenvironment, particularly the area around fluorophore functional groups [40]. Structural changes of BSA by varying the concentration of ruthenium(II) hydrazone complexes were recorded as a function of  $\Delta\lambda = 15$  and  $\Delta\lambda = 60$  nm and are given in figure 7(a) and (b).

When the concentrations of **1** and **2** added to BSA were increased, the tyrosine intensities were reduced to a small extent of about 14 and 9.6%, respectively, but tryptophan intensities were decreased about 50 and 41.58%, respectively. Though, the complexes affected tyrosine and tryptophan microenvironments, the effect was more prominent in tryptophan residue than tyrosine microenvironment. The interaction of ruthenium(II) hydrazone complexes with tyrosine and tryptophan residues led to a decrease in the polarity of the fluorophore by increasing the hydrophobicity around the same. The features of synchronous measurements confirmed the changes in the conformation of BSA upon interaction with the complexes.

### 3.5. In vitro cytotoxicity

Ruthenium(II) hydrazone complexes **1** and **2** were evaluated against HeLa and MCF-7 cell lines by MTT assay and the activity corresponding to inhibition of cancer cell growth at maximum level is shown in figures S6–S8. Table 3 shows the  $IC_{50}$  values of the complexes and control. The results reveal that the complexes possess significant cytotoxic potencies

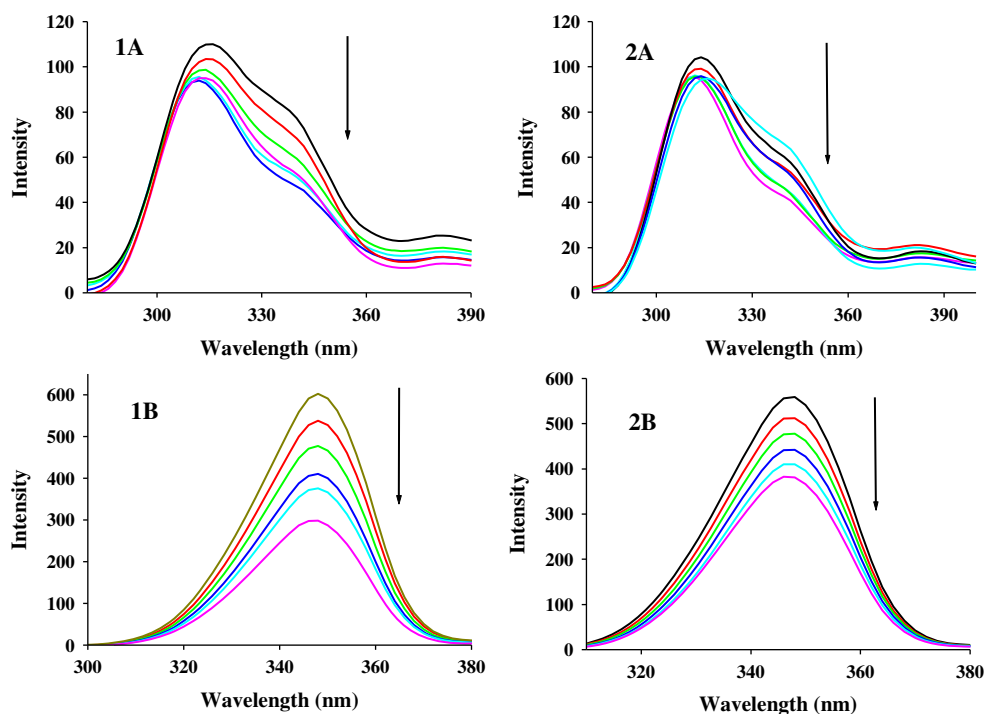


Figure 7. Synchronous spectra of BSA ( $1 \times 10^{-6}$  M) as a function of concentration of **1** and **2** (0, 2, 4, 6, 8,  $10 \times 10^{-7}$  M) with wavelength difference of  $\Delta\lambda = 15$  nm (1A and 2A) and 60 nm (1B and 2B).

Table 3. IC<sub>50</sub> (μM) concentration of ruthenium(II) hydrazone complexes.

Complex	HeLa	MCF-7
<b>1</b>	18.0 ± 0.5	2 ± 1
<b>2</b>	21.0 ± 0.6	6 ± 1
Cisplatin	53.0 ± 0.7	10 ± 2

with IC<sub>50</sub> values in the very low micromolar concentrations and are superior to commercial drug cisplatin (not shown in graph). The compounds tested herein showed better cytotoxicity than the complexes [Ru(bpy)<sub>2</sub>(L1)](PF<sub>6</sub>)<sub>4</sub>·CH<sub>3</sub>OH (IC<sub>50</sub> = 452 ± 22 μM) and [Ru(bpy)<sub>2</sub>(L2)](PF<sub>6</sub>)<sub>4</sub>·2H<sub>2</sub>O (IC<sub>50</sub> = 419 ± 17 μM) against HeLa cell lines [44]. Similarly, **1** and **2** exhibited significant cytotoxicity against MCF-7 cell lines, comparable or even better than that of [RuCl(CO)(PPh<sub>3</sub>)(L2)] (IC<sub>50</sub> = 3.2 ± 0.3 μM) and a series of ruthenium(II)-β-carboline complexes (IC<sub>50</sub> = 50 μM) [45, 46].

Regarding the comparative efficiency of **1** and **2** on the cell lines used in this study, proliferation of both of them was arrested to a greater extent by **1** with predominant damage to MCF-7 compared to the other cell line.

Among the two complexes, **1** possessing thiophene ring in the ligand assembly showed more effectiveness than **2** containing furan ring in the ligand part against both the tested cell lines. The findings of *in vitro* anticancer activities further proved binding of the complexes to DNA caused cell death.

#### 4. Conclusion

Syntheses of [RuH(CO)(L<sup>1</sup>)(PPh<sub>3</sub>)<sub>2</sub>] (**1**) and [RuH(CO)(L<sup>2</sup>)(PPh<sub>3</sub>)<sub>2</sub>] (**2**) containing N,O-donating heterocyclic hydrazones with significant biomolecular interactions and *in vitro* cytotoxicities are described. Proof for the nature of coordination of HL<sup>1</sup> in **1** was derived from single crystal XRD analysis. The complexes were DNA-intercalators based on the UV-vis spectral titrations, EB-displacement fluorescence quenching studies, and viscosity measurement studies in the presence of CT-DNA. Fluorescence quenching of **1** and **2** with BSA showed a strong interaction and their modes of quenching using absorption spectroscopy were by static quenching. Among the tyrosine and tryptophan microenvironments of BSA, both complexes showed preferential interaction around the tryptophan of BSA. *In vitro* cytotoxicity of the complexes against HeLa and MCF-7 cell lines authenticated that **1** containing sulfur in its hydrazone displayed better performance than **2** containing oxygen. The observed cytotoxic potentials of **1** and **2** are superior to other ruthenium(II) complexes reported and standard anticancer drug cisplatin.

#### Supplementary material

CCDC deposition No. 1024327 contains the supplementary crystallographic data for **1**. These data can be obtained free of charge via <http://www.ccdc.cam.ac.uk/conts/retrieving>.

[html](#), or from the Cambridge Crystallographic Data Center, 12 Union Road, Cambridge CB2 1EZ, UK; Fax: +44 1223-336-033; or E-mail: [deposit@ccdc.cam.ac.uk](mailto:deposit@ccdc.cam.ac.uk).

## Disclosure statement

No potential conflict of interest was reported by the authors.

## Funding

The authors would like to extend their sincere appreciation to the Deanship of Scientific Research at King Saud University for its funding to this Research Group No. (RG 1435-001).

## Supplemental data

Supplemental data for this article can be accessed <http://dx.doi.10.1080/00958972.2015.1077950>.

## References

- [1] T. Boulikas. *Cancer Ther.*, **5**, 351 (2007).
- [2] G.B. Jiang, X. Zheng, J.H. Yao, B.J. Han, W. Li, J. Wang, H.L. Huang, Y.J. Liu. *J. Inorg. Biochem.*, **141**, 170 (2014).
- [3] Y.Y. Xie, H.L. Huang, J.H. Yao, G.J. Lin, G.B. Jiang, Y.J. Liu. *Eur. J. Med. Chem.*, **63**, 603 (2013).
- [4] Y.K. Yan, M. Melchart, A. Habtemariam, P.J. Sadler. *Chem. Commun.*, **38**, 4764 (2005).
- [5] J.M. Rademaker-Lakhai, D.V.D. Bongard, D. Pluim, J.H. Beijnen, J.H.M. Schellens. *Clin. Cancer Res.*, **10**, 3717 (2004).
- [6] C.G. Hartinger, S.Z. Seifried, M.A. Jakupec, B. Kynast, H. Zorbas, B.K. Keppler. *J. Inorg. Biochem.*, **100**, 891 (2006).
- [7] F. Gümüş, G. Eren, L. Açık, A. Çelebi, F. Öztürk, S. Yılmaz, R.I. Sağkan, S. Gür, A. Özkul, A. Elmalı, Y. Elerman. *J. Med. Chem.*, **52**, 1345 (2009).
- [8] M. Alagesan, N.S.P. Bhuvanesh, N. Dharmaraj. *Eur. J. Med. Chem.*, **78**, 281 (2014).
- [9] U. Katrahalli, V.K.A. Kalalbandi, S. Jaldappagari. *J. Pharm. Biomed. Anal.*, **59**, 102 (2012).
- [10] U. Katrahalli, U.S. Jaldappagari, S.S. Kalanur. *J. Lumin.*, **130**, 211 (2010).
- [11] D. Senthil Raja, N.S.P. Bhuvanesh, K. Natarajan. *Dalton Trans.*, **41**, 4365 (2012).
- [12] M. Alagesan, N.S.P. Bhuvanesh, N. Dharmaraj. *Dalton Trans.*, **43**, 6087 (2014).
- [13] K. Prashant, K.G. Rakesh, S.P. Daya. *Chem. Soc. Rev.*, **43**, 707 (2014).
- [14] N. Ahmed, J.J. Levison, S.D. Robinson, M.F. Uttley. *Inorg. Synth.*, **15**, 48 (1974).
- [15] M.S. Rao, K.H. Reddy. *Indian J. Chem.*, **38A**, 262 (1999).
- [16] APEX2, Program for Data Collection on Area Detectors, BRUKER AXS Inc., Madison, WI (2007).
- [17] Sheldrick G.M., SADABS. Program for Absorption Correction of Area Detector Frames, BRUKER AXS Inc., Madison, WI (2008).
- [18] G.M. Sheldrick. *Acta Crystallogr., Sect. A: Found. Crystallogr.*, **64**, 112 (2008).
- [19] O.V. Dolomanov, L.J. Bourhis, R.J. Gildea, J.A.K. Howard, H. Puschmann. *J. Appl. Cryst.*, **42**, 339 (2009).
- [20] M.F. Reichmann, S.A. Rice, C.A. Thomas, P. Doty. *J. Am. Chem. Soc.*, **76**, 3047 (1954).
- [21] J.B. Chaires, N. Dattagupta, D.M. Crothers. *Biochemistry*, **21**, 3933 (1982).
- [22] M. Titas, M. Manjira, S. Buddhadeb, B. Snehasis, H. Geeta, C. Pabitra. *J. Coord. Chem.*, **67**, 2643 (2014).
- [23] C. Rajput, R. Rutkaite, L. Swanson, I. Haq, J.A. Thomas. *Chem. Eur. J.*, **12**, 4611 (2006).
- [24] N. Selvakumaran, N.S.P. Bhuvanesh, R. Karvembu. *Dalton Trans.*, **43**, 16395 (2014).
- [25] T. Mosmann. *J. Immunol. Methods*, **65**, 55 (1983).
- [26] M. Muthukumar, P. Viswanathamurthi. *J. Coord. Chem.*, **63**, 1263 (2010).
- [27] R. Karvembu, K. Natarajan. *Polyhedron*, **21**, 1721 (2002).
- [28] M. Alagesan, N.S.P. Bhuvanesh, N. Dharmaraj. *Dalton Trans.*, **42**, 7210 (2013).
- [29] P. Krishnamoorthy, P. Sathyadevi, R.R. Butorac, A.H. Cowley, N. Dharmaraj. *Metallomics*, **4**, 498 (2012).
- [30] N. Chitrapriya, V. Mahalingam, M. Zeller, H. Lee, K. Natarajan. *J. Mol. Struct.*, **984**, 30 (2010).
- [31] J.G. Małecki. *Polyhedron*, **29**, 2489 (2010).
- [32] J.G. Małecki, A. Maron. *Polyhedron*, **44**, 221 (2012).

- [33] D. Senthil Raja, N.S.P. Bhuvanesh, K. Natarajan. *Eur. J. Med. Chem.*, **47**, 73 (2012).
- [34] B.C. Baguley, M. Le Bret. *Biochemistry*, **23**, 937 (1984).
- [35] H. Paul, T. Mukherjee, M. Mukherjee, T.K. Mondal, A. Moirangthem, A. Basu, E. Zangrando, P. Chattopadhyay. *J. Coord. Chem.*, **66**, 2747 (2013).
- [36] D. Suh, J.B. Chaires. *Bioorg. Med. Chem.*, **3**, 723 (1995).
- [37] J.L. Butour, J.P. Macquet. *Biophys. Acta Nucleic Acids Protein Synth.*, **653**, 305 (1981).
- [38] M. Shilpa, C. Shobha Devi, P. Nagababu, J.N.L. Latha, R. Pallela, V.R. Janapala, K. Aravind, S. Satyanarayana, *J. Coord. Chem.*, **66**, 1661 (2013).
- [39] D. Senthil Raja, G. Paramaguru, N.S.P. Bhuvanesh, J.H. Reibenspies, R. Renganathan, K. Natarajan. *Dalton Trans.*, **40**, 4548 (2011).
- [40] P. Sathyadevi, P. Krishnamoorthy, R.R. Butorac, A.H. Cowley, N.S.P. Bhuvanesh, N. Dharmaraj. *Dalton Trans.*, **40**, 9690 (2011).
- [41] P. Sathyadevi, P. Krishnamoorthy, N.S.P. Bhuvanesh, P. Kalaiselvi, V. Vijaya Padma, N. Dharmaraj. *Eur. J. Med. Chem.*, **55**, 420 (2012).
- [42] A. Tarushi, X. Totta, A. Papadopoulos, J. Kljun, I. Turel, D.P. Kessissoglou, G. Psomas. *Eur. J. Med. Chem.*, **74**, 187 (2014).
- [43] J. Kljun, I. Bratsos, E. Alessio, G. Psomas, U. Repnik, M. Butinar, B. Turk, I. Turel. *Inorg. Chem.*, **52**, 9039–9052 (2013).
- [44] J. Sun, W.X. Chen, X.D. Song, X.H. Zhao, A.Q. Ma, J.X. Chen. *J. Coord. Chem.*, **68**, 308 (2015).
- [45] S. Selvamurugan, P. Viswanathamurthi, A. Endo, T. Hashimoto, K. Natarajan. *J. Coord. Chem.*, **66**, 4052 (2013).
- [46] Y. Chen, M.Y. Qin, J.H. Wu, L. Wang, H. Chao, L.N. Ji, A. Xu. *Eur. J. Med. Chem.*, **70**, 120 (2013).